Study of fluctuations of electric and aerosol characteristics of the atmosphere as a precursor of tectonic activity

G.G. Matvienko, V.A. Alekseev,* A.I. Grishin, G.M. Krekov, and M.M. Krekova

Institute of Atmospheric Optics, Siberian Branch of the Russian Academy of Sciences, Tomsk
** Institute of Innovation and Thermonuclear Investigations, Troitsk*

Received March 7, 2007

The results of combined investigation into fluctuations of electric and aerosol characteristics of the atmosphere as a precursor of tectonic activity of the Earth's crust are presented. Experimental measurements were conducted near the Bugaz Fault at the Taman Peninsula. It is shown that the absolute values of the electric field strength E and the aerosol scattering coefficient σ_s begin to increase several hours before an earthquake and decrease to the background values immediately after an earthquake shock. The shape and maxima of the amplitude spectra of E and σ_s depend on the time interval between the measurement and the tectonic disturbance. The data obtained show that aerosol significantly affects the electric characteristics of the atmosphere. Optical and meteorological conditions, under which aerosol inversions of the seismic origin can be found with the aid of an orbital lidar, were determined in the numerical Monte Carlo experiment.

Introduction

Earthquakes were and are the largest natural cataclysms associated with the mass mortality of people and significant destruction of the infrastructure. The most known catastrophic earthquakes took place in California (1906), Ashkhabad (1948), Spitak (1988), Alaska (1964), Iran (1990), Pakistan (2003), and Indonesia (2006). Statistically, every year 20 earthquakes with the magnitude $M > 7$, 100–120 potentially dangerous earthquakes with $M > 5$, and 300 000 small earthquakes take place. Therefore, the search for new earthquake precursors and development of theory for earthquake prediction are quite urgent problems. Earthquake precursors are various physical phenomena observed several hours or days before the earthquake shock, for example, variations of geophysical fields, anomalous behavior of animals, and others, which allow the main problem of prediction to be solved, namely, to predict the place, time, and magnitude of a seismic event. The solution of this problem requires the development of reliable methods for monitoring of earthquake precursors, revealing of their nature, creation of adequate models describing these precursors, and development of the efficient earthquake prediction strategy.

1. State of the art and promises for the problem solution

Recent investigations indicate clearly the existence of a relation between processes in the Earth's lithosphere and atmospheric and ionospheric perturbations. It is well known that numerous anomalous variations of fields and parameters of the atmosphere and the near-Earth space are observed at different stages of development of tectonic processes. Analysis of peculiarities of these variations along with traditional methods of geophysical prediction form the bases for development of methods of the short-term earthquake prediction. Specific effects of seismic origin manifesting themselves in the ionosphere are studied intensively for several decades.[1–6,10,11] Anomalous variations of the ionosphere associated with earthquakes are observed with different aids of the radiophysical monitoring. For this purpose, measurements of ground-based vertical ionospheric sensing stations are used, as well as orbital ionosondes installed at satellites, such as, for example, ISIS-2, AUREOL-3, ALOUETTE, INTERKOSMOS-19, EOS (Aqua and Terra), ENVISAT, and other spacecrafts.[7–9,10,11]

As was shown in Ref. 6, seismoionospheric earthquake predictors show themselves as deviations of the density of ionospheric plasma from the unperturbed state. They are observed during several days or hours before earthquakes with the magnitude $M > 5.0$. These variations mostly have amplitude of 15–25%, sometimes achieving 100%. The launch and development of the GPS and GLONASS satellite navigation systems, creation of specialized projects (ESPERIA, KOMPAS-2)[10,11] aimed at prediction of earthquakes and volcanic eruptions, and fast progress of the global network of GPS stations started the new stage in the study of ionospheric variations observed before and after strong earthquakes.

However, the solution of the problem cannot be based only on the analysis of one class of ionospheric phenomena, because there remains a probability of

0235-6880/07/08 629-09 $02.00

the final false decision. The reason is that geomagnetic perturbations caused by the solar activity and the state of the interplanetary environment usually[10] significantly exceed and, consequently, mask weak seismoionospheric effects. Though the latter ones have some phenomenological features,[6] strict quantitative criteria of making a decision on a possible earthquake are absent at the present time. Nevertheless, this field of investigations is considered as most promising, and a new group of ionospheric satellites,[29] namely, DEMETER, SICH-1M, and TIMED, will be orbited in the nearest future. It is believed that the modernized instrumentation installed on these satellites will allow the regular monitoring of seismoionospheric manifestations.

The accuracy of prediction can be improved due to the combined approach by revealing and analyzing alternative earthquake predictors. Thus, the anomalous increase in the intensity of low-frequency radio waves over epicenters of earthquakes with $M > 5.0$ was found from the GEOS-1 and GEOS-2 satellites. Papers were published,[29] which demonstrate the correlation between the seismic activity and variations in flow of charged particles captured by the geomagnetic field. A new method for earthquake prediction based on the lineament analysis of space images of seismic territories was proposed recently.[34]

In the recent time, the interest to capabilities of optical methods for remote sensing of anomalous atmospheric phenomena accompanying the development of catastrophic tectonic processes in the lithosphere has increased. Several promising researching fields have been formed, first of all, investigations with the use of systematic data of satellite measurements of the IR radiation outgoing from the seismic areas of the Earth's surface.[13–16] Tronin in his papers[13,14] has demonstrated a correlation between thermal anomalies on the Earth's surface and the seismic activity. In China, this method is now implemented in the practice of actual monitoring.[23] However, the mechanism of appearance of such anomalies[15] and the reliability of their identification, especially, under the conditions of meteorological instability of the atmosphere remain open questions yet.

Interesting methodical results are obtained by scientists of the Abastuman Astrophysical Observatory in the optical wavelength region.[17] They found that in the central Asia in the lower ionosphere, namely, in the E layer (85–110 km) over the epicenter, the OI emission intensity in the lines at 557.7 and 630.0 nm increased several hours before the beginning of an earthquake. Within the framework of the "Space-US" International Program (Russia – Belarus),[18] a small-sized spectral photometric system was designed for observation of the emission of atomic oxygen in the scheme of limb measurements from a board the ISS. The system includes a module for measurement of the spectral intensity of hydroxyl (OH) in the range 830–1040 nm. Intensity variations reflect the character of behavior of internal gravitational waves.

The statistics of both ground-based[12,19,22,25] and orbital[20,21] observations in the recent years shows that the development of an earthquake is accompanied by a number of anomalous deviations of optical and meteorological parameters in epicentral areas: weather changes drastically, atmospheric pressure drops, low-lying cloudiness of unusual configuration and dynamics appears (one of the oldest predictors),[22,28] temperature and humidity of the near-surface atmosphere increase,[20,22,25] the O_3 content varies sharply,[26,29] emissions of Ra [Refs. 24, 25, 27] and other trace and greenhouse gases (CH_4, CO_2, CO, H_2S, SO_2, HCl) are observed. The EOS and ENVISAT modern satellite systems are capable of measuring the CO and CH_4 concentration in the atmosphere, but published data are unavailable yet. The SeaWiFS multichannel spaceborne module[30] has recorded anomalous aerosol formations in the process of earthquake development in Southwestern India (January, 2001).[21] Ground-based contact measurements[12,19] confirm that the increase in the concentration of mineral metal-containing particles is observed several hours before first destructive shocks.

Among remote methods of monitoring of the mentioned optical and meteorological parameters of the atmosphere, laser sensing methods are characterized by the highest speed and the highest spatial resolution.[30] The laser method for remote monitoring of the near-surface radon content should be noted to be promising as one of the most important earthquake precursors.[33]

Airborne laser sensing systems have shown a rather high efficiency in solution of some problems of meteorology, ecology, atmospheric and ocean physics.[31,32] Deployment of such systems at orbital stations and satellites significantly extends the capabilities of monitoring, making it global and systematic. We speak about the real-time monitoring of the spatial field of main atmospheric parameters, including cloud fields, vertical structure of the aerosol and gas composition of the troposphere, ecologically dangerous local-scale emissions, and, finally, possible earthquake predictors. At the same time, airborne and stationary lidars keep their role as important instruments of the subsatellite monitoring.

Methodologic aspects of the problem of laser sensing of the atmosphere from space were analyzed still in early papers.[35,36] To date, some projects are technically implemented.[37,38] In particular, in 1995 a cycle of investigations was carried out with the BALKAN Russian Spaceborne Lidar installed at the MIR Orbital Station. The ALISSA Russian–French Lidar as a part of the PRIRODA Module of the same station was orbited in May, 1996. In September, 1994 the first quite successful experiment on the multifrequency laser sensing throughout the Earth's atmosphere depth was conducted from aboard the Shuttle spacecraft.[39] This orbital experiment was

accompanied by a series of ground-based and airborne lidar sensing.

The encouraging effectiveness of the first lidar space experiments on investigation of cloud fields, profiles of aerosol characteristics, and some parameters of the surface formulates the next stage of the problem of introducing this class of space lidars into the system of monitoring observations of the Earth. Thus, the Program of the Etalon Russian Space Agency included some projects oriented at development of a network of small specialized satellites for detection of regions of possible seismic cataclysms by one class of precursors. Since the increased concentration of the coarse mineral aerosol fraction in the boundary atmospheric layer is an important earthquake precursor,[12,19,21] it was supposed to equip one satellite of this network, namely, TECTONICA-A with a multifrequency lidar operating in a long-term automated mode.[40–42] An alternative variant is presented by an idea[43] to create a multipurpose power-consuming satellite equipped with seismic detectors of different types (electric, magnetic, optical, etc.). All these approaches require *a priori* development within the field and theoretical simulation.

2. Experimental investigations into fluctuations of electric and aerosol characteristics of the atmosphere in regions with tectonic activity

2.1. Selection of a region for experimental investigations

Deformation of the Earth's crust causes changes in fluid and aerosol flows and activates seismic processes. Tectonic aerosols in the atmosphere are condensation nuclei causing the formation of clouds along faults, which was many times observed in space images.[14] Thus, the increase in the aerosol background caused by the appearance of aerosol particles entrained by the gas flow (H_2, He_2, CO_2, CH_4, etc.) into the atmosphere through near-surface microcracks is a sign of intensification of the tectonic activity. Changes are observed in the concentration, size spectrum, and chemical composition of aerosol particles.[12,13,16,19] The dynamics of concentration of such an aerosol can be detected and measured remotely in real time with the aid of the laser sensing technique. It is interesting to note[44] that the intense aerosol emission of the Avacha Volcano, Kamchatka, in December, 1990 was a sole reliable precursor of the following earthquake, because the data of geophysical monitoring based on seismograms gave no observable indications.

At the same time, the aerosol component causes changes in the Earth's electric field, which also can be an indicator of variability of the tensometric characteristics of the Earth's crust. The selection of Earth's electrostatic characteristics as possible earthquake signs is caused also by the fact that anomalies of the geoelectric field are known to correlate with the increased concentration of gases, first of all, radon in the subsoil levels and in the atmosphere upon crust deformation in earthquake source areas.[46–48] In Refs. 20, 24, 29, and 48, it was noted that the radon and aerosol earthquake signs coincide in time. In addition, in the presence of conducting aerosol particles, the ionization activity of radon increases sharply, and, consequently, the electric field strength increases many times. Possible models of kinetics of atmospheric gases and particulates in the presence of radioactive radon are actively discussed in the literature.[24,29]

Based on these prerequisites, in October, 1999 the research mission was carried out on the Taman Peninsula near the Bugaz Fault. This region is selected because it lies in the seismically active zone with progressing mud volcanism, extending from Crimea to the Central Asia, where we carried out our investigations.[45] Soil degassing along and across the fault is inhomogeneous, and therefore, to reveal the most active areas in the Bugaz Fault, we used a microlidar designed for Mars aerosol measurements.[54] Areas with the maximal activity of aerosol emissions were revealed. It was found in the process of survey that aerosol flows on the fault axis and outside the fault differ by more than an order of magnitude.

During the mission, the hydrogen mapping along and across the fault was carried out; the hydrogen concentration in the near-surface layer ranged within 2.6–3.7 ppm. This fact, in addition to the lidar measurements, has allowed us to refine the selection of the optimal area, at which we measured the aerosol scattering coefficient, the electric field strength, and the electric conductivity of the atmosphere. Analogous investigations were carried out in an adit near Novorossiisk, were permanent observations of degassing are conducted. The seismic situation in the Krasnodarskii Krai is recorded at the Anapa Seismic Station.

2.2. Analysis of experimental results

During the mission, the following physical characteristics were measured:

– strength of the atmospheric electric field with the aid of a dynamic-type sensor converting the direct field of the Earth into the alternating one[46];

– electric conductivity of the atmospheric air, measured from the discharge time of an open mesh capacitor;

– volume aerosol scattering coefficient with the aid of a small-sized aerosol sensor measuring the radiation scattered at an angle of 45°.

Measurement devices were connected to the Notebook computer, responsible for acquisition of experimental data and their primary statistical processing. Later on, the temporal characteristics of measured parameters were analyzed. For the aerosol scattering coefficient and the electric field strength,

we analyzed also the amplitude spectra obtained with the aid of standard preparatory procedures through the Fourier transform.[51] The spectral analysis was applied to two types of time series, the first characterized by the complete absence of shocks and the second including the time period immediately before an earthquake.

The analysis of temporal electric and optical characteristics of the atmosphere revealed fluctuations of signals coinciding in time with earthquake shocks. Figure 1 shows the temporal behavior of the aerosol scattering coefficient and the electric field strength for the period of October 19–22, 1999.

The investigation of spectral characteristics of fluctuations of the aerosol scattering coefficient σ_s has shown that they significantly depend on the activity of the Earth's crust during measurements. Figure 2 shows the power density spectra of fluctuations of the σ amplitude drawn for the "calm" period and in the period immediately before some earthquake. The analysis of these data shows that the maximal values of the spectra of amplitude fluctuations fall on the period before the earthquake, and the maxima differ more than twice. In addition, the amplitude spectrum of σ fluctuations for the active period is characterized by a wider variability of $S_\sigma(f)$.

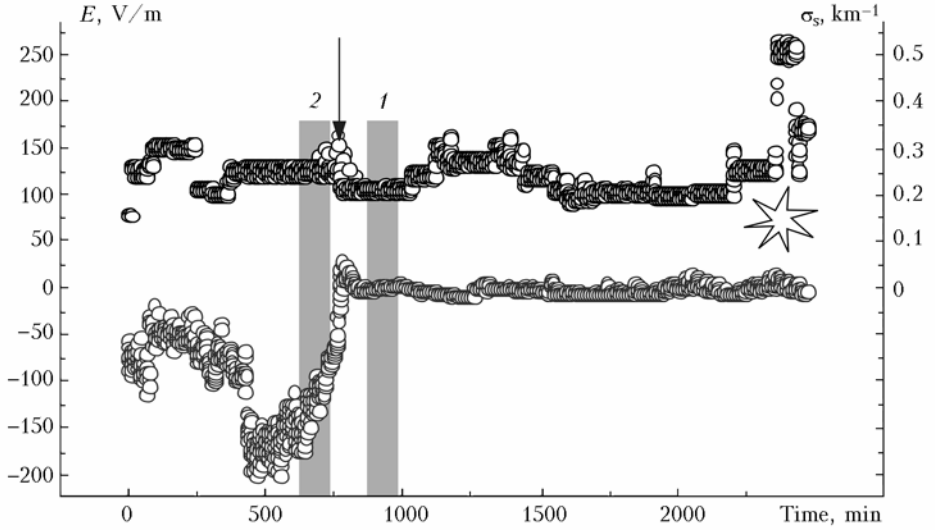

Fig. 1. Time dependence of the electric field strength E (lower circles) and the scattering coefficient σ_s (upper circles). The arrow indicates the time of earthquake, the asterisk shows the time of explosion during adit measurements: (*1*) measurements in the absence of quake, (*2*) immediately before an earthquake.

The arrow shows the time, at which the local seismic station detected the earthquake shock with the magnitude $M = 4.5$ and the epicenter 450 km far from the Anapa Seismic Station. The asterisk corresponds to adit observations, when 500 kg of ammonite were exploded 300 m far from the measurement site. One can see from the curves that the electric field strength E significantly increased in the absolute value up to about 170 V/m several hours before the earthquake. Then, immediately before the shock, the value of E decreased fast to the background level. The scattering coefficient for this period increased roughly by 50% and remained nearly constant until the shock, after which it returned to the former level.

It is interesting that the quake caused by the technogenic reason (explosion in an open-cast mine) did not affect significantly the temporal behavior of E. At the same time, the quake caused the fall of dust from adit walls, which resulted in the increase of the aerosol scattering coefficient after the explosion.

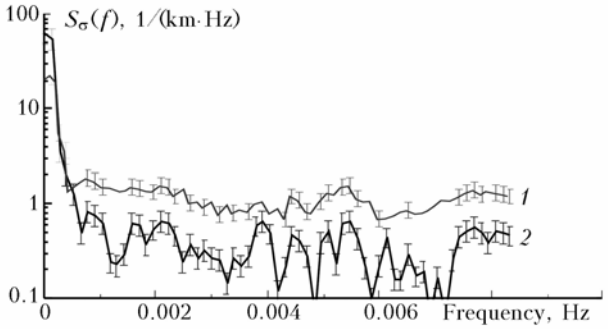

Fig. 2. Amplitude spectra of fluctuations of the scattering coefficient σ_s in the calm period (*1*) and before the earthquake (*2*). Vertical bars indicate the confidence interval for the 0.9 probability.

The spectra of fluctuations of the electric field strength $S_E(f)$ also significantly depend on the period of measurements. Figure 3 shows the spectra of fluctuations of the E amplitude for the periods of the "calm" crust and before an earthquake.

One can see that the maximal values of the spectra of amplitudes for the different situations differ more than tenfold! So high difference demonstrates that tectonic processes in the crust play rather significant role in formation of the electric field structure in this region. Figure 4 shows the temporal behavior of the atmosphere electric conductivity.

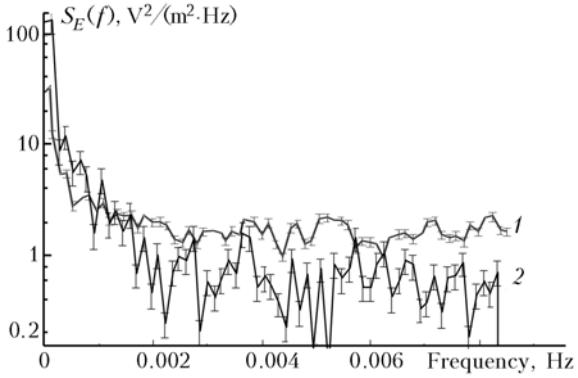

Fig. 3. Amplitude spectra of fluctuations of the electric field strength E in the calm period (*1*) and before the earthquake (*2*). Vertical bars indicate the confidence interval for the 0.9 probability.

Shocks are preceded by the increase in the atmospheric conductivity, which can be explained by the increase in the concentration of charged particles in the air. From comparison of Figs. 1 and 4 we can see that both the scattering coefficient and the electric conductivity of the atmosphere increase immediately before the shock. Therefore, there arises a question on the correlation between the aerosol and electroconductive properties of the atmosphere. The influence of aerosol on the concentration of charged particles n can be approximately estimated from the following equation[52]:

$$\frac{dn}{dt} = \nu - \alpha n^2 - \beta N n,$$

where ν is the intensity of ion formation; α is the recombination coefficient; β is the coefficient of attachment of light ions to aerosol particles; N is the concentration of aerosol particles. For the equilibrium state at $dn/dt = 0$, the differential equation transforms into the second-order equation, which can be easily solved for n. It follows from the solution that the influence of aerosol particles on the ion concentration is significant at $\beta N \gg \alpha\nu$. This condition always fulfills in the surface atmosphere, and therefore the aerosol component should be taken into account in calculations of electrostatic characteristics of the atmosphere. In addition, it follows from the analysis of statistical data of many-year measurements of atmosphere electric characteristics that with time the electric conductivity of the atmosphere decreases slowly, which is attributed to the increasing concentration of anthropogenic aerosol.[53] Since the inverse process is observed in our case, we can conclude that a significant amount of ions is emitted into the atmosphere.

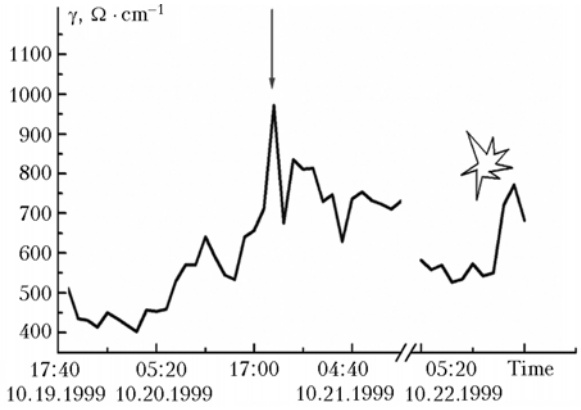

Fig. 4. Time dependence of the atmospheric conductivity γ in October 19 to 22. The arrow indicates the time of earthquake, the asterisk shows the time of explosion during adit measurements.

3. Numerical experiment on sensing of aerosol inversions in the boundary atmospheric layer with the use of orbital lidar

Below we present the results of the numerical experiment aimed at the study of potential capabilities of an orbital lidar in detection and identification of aerosol inversions of the seismic origin in the atmospheric boundary layer. The calculations were performed through the solving the nonstationary transport equation by the Monte Carlo technique. The technique allows estimation of signals with separation by the number of interactions and the angles of arrival of photons to a detector. This forms the basis for a detailed analysis of the lidar signal structure depending on optical and geometrical conditions of the experiment.

The transport equation is solved for the initial and boundary conditions corresponding to the functional scheme of the TECTONICA-A spaceborne lidar.[40–42] It is assumed that the lidar is spaced by H_0 from the Earth's surface, and the source emits isotropically in a cone $2\pi(1 - \cos\varphi_i)$, where φ_i is the divergence angle. The reflected signal is recorded by the receiver in the angular cone $2\pi(1 - \cos\varphi_d)$ bounded by the detector aperture φ_d. The main specifications of the lidar necessary for estimation are presented below.

Orbit altitude H_0, km	400–600
Operating wavelengths λ_i, μm	1.064, 0.532, 0.355
Beam divergence φ_i, mrad	1.0, 0.4, 0.4
Pulse duration τ_i, ns	27, 27, 30
Detector aperture φ_d, mrad	1–20
Spatial resolution Δh, km	0.1– 1

The wide range of the field of view (up to 20 mrad) is caused by the supposition that a multicell receiving mirror will be deployed in space.[42]

It should be only noted that the used mathematical algorithms[55,56] allow calculation of the spatiotemporal transformation of an optical signal under the conditions maximally close to real ones. This implies a possibility to take into account the multicomponent composition of the atmosphere up to altitudes $h = 90$ km in the approximation of a detailed stratified-inhomogeneous model. The optical properties of the scattering medium are described by the scattering phase function $g(\vartheta)$, the extinction coefficient $\sigma_{ext}(h)$, and the quantum survival probability $\Lambda(h)$. In calculations, these characteristics are specified for the required set of wavelengths according to the background model,[57] based on the averaging of numerous statistical data on the concentration and microphysical properties of the atmospheric aerosol.

When extracting information from the results of laser sensing of a scattering medium, it is necessary to have a rather complete idea on, first of all, the structure of a lidar signal depending both on variations of optical properties of the medium and on the geometry of the transceiving system. In addition, it is necessary to estimate the expected noise level of the multiple-scattered radiation under different extreme, from the viewpoint of optical weather, situations. In this paper, we present the results of calculations concerning these basic problems of lidar sensing. All estimates were obtained for a lidar orbiting at an altitude $H_0 = 400$ km relative to the Earth's surface.

For convenient scaling, the time scans of the relative scalar intensity of the reflected signal are presented in Fig. 5 for limited height ranges starting from the ground ($h = 0.0$ km). Figure 5*a* shows the vertical profiles of the extinction coefficients including molecular scattering and absorption by ozone, while Figures 5*b* and *c* show the profiles of backscattering signals $P(h)$ for the operating wavelengths of the garnet laser.

The results indicate possible problems with the detection of IR signals under the conditions of the clear cloudless atmosphere. The structure of the signal $P(h)$ is depicted in Fig. 5*c* for $\lambda = 0.35$ and 1.06 μm. The results of calculation of different functionals are presented in Fig. 5 as functions of h, which is equivalent to the accumulated track or the time of a photon residence in a given angular interval in the scattering medium; $h = ct/2$, where c is the speed of light. The functional histograms are constructed with the averaging in the gating interval $\Delta h = 0.5$ km up to a height of 3 km above the ground and higher with the interval $\Delta h = 0.1$ km.

At the background state of the aerosol atmosphere, the reflected signal $P(h)$ at $\lambda = 0.35$ μm is almost completely determined by the molecular-scattered radiation. The aerosol component of the signal becomes comparable with the molecular one only in the lower troposphere up to an altitude of about 0.2 km. As the wavelength increases up to 1.06 μm, the aerosol component of the signal becomes decisive in $P(h)$ starting from an altitude of 4–5 km above the ground.

One of the purposes of the TECTONICA-A spaceborne lidar system is the detection and prediction of natural and anthropogenic cataclysms accompanied by extreme emissions of aerosol in the lower troposphere. In particular, from the measurements conducted in Guadalajara (Mexico)[12,19] during the earthquake of October 9, 1995, it follows that several hours before the first shock the number concentration of the coarse fraction of aerosol particles in the boundary atmospheric layer increased markedly (1.5–2 times). In the particulate composition, the increased content of Si, Ca, and Fe was observed, which is characteristic of the minerals emitted from the surface and, possibly, from the depth.

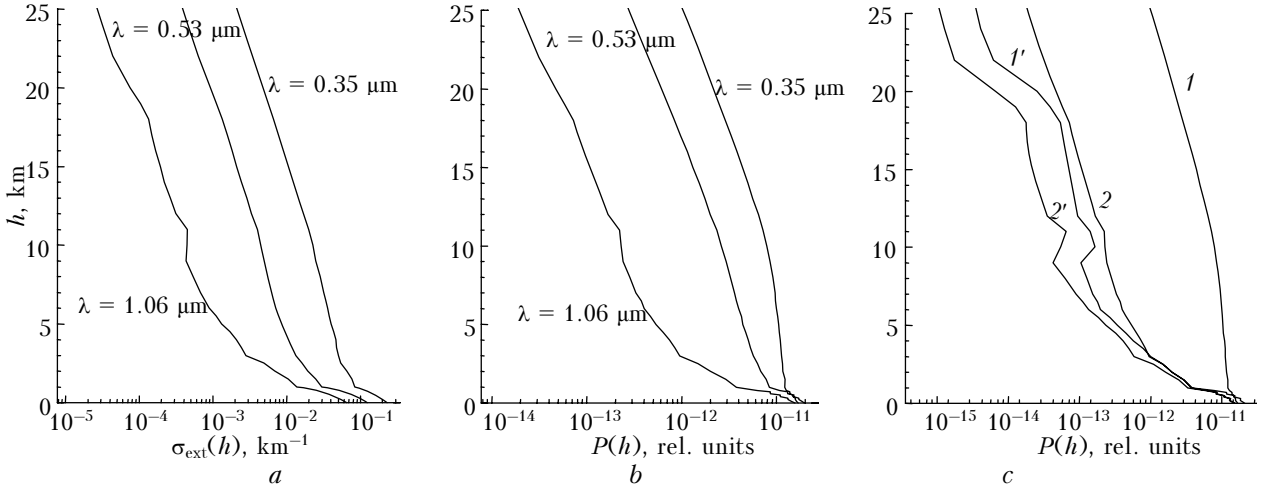

Fig. 5. Vertical profiles of the extinction coefficient $\sigma_{ext}(h)$ for the used wavelengths of laser sensing (*a*); estimate of the reflected signal $P(h)$ for the lidar with the detection angle $\varphi_d = 10$ mrad (*b*); (curves *1′*, *2′*) are the aerosol components of $P(h)$ of the signal at wavelengths of 0.35 and 1.06 μm, respectively, (*1*, *2*) total signal (*c*).

The Table[19] represents the dynamics of the particle size spectrum in the surface atmosphere during the development of the earthquake in Guadalajara. The data presented are the related concentrations of particles of different size $\Delta N d_i / \overline{\Delta N} d_i$ in percent, normalized to the mean concentration measured earlier under stable meteorological conditions. To be noted is the sharp, to nearly zero, decrease in the concentration of the fine fraction of particles with the diameter $0.4 \le d \le 0.5$ μm. After the first shock, the concentration of the coarse fraction of mineral particles with the diameter $d \ge 1.0$ μm increased catastrophically.

d_i, μm	October 8				October 9		
	21:00	22:00	23:00	24:00	9:20	10:10	11:00
>10	73	81	88	136	579	684	263
10–7	100	139	65	125	544	596	772
7–4	67	144	152	122	237	204	51
4–2	64	102	140	131	281	324	234
2–1,5	64	136	153	137	129	150	296
1.5–1.0	76	157	166	126	118	495	75
1.0–0.9	97	145	95	102	101	118	63
0.9–0.8	68	143	82	229	63	251	190
0.8–0.7	149	193	163	90	133	170	174
0.7–0.6	101	143	132	106	100	96	80
0.6–0.5	120	71	103	99	77	88	60
0.5–0.4	90	36	89	42	0	0	0
0.4	108	105	123	98	92	115	93

The results of Refs. 12, and 19 are unique, they are of undoubted interest, and we used them in the numerical experiment. The transformed spectra of aerosol particles have allowed us to recalculate the necessary parameters of aerosol light scattering. We proposed that the area of increased tropospheric turbidity reaches the height $h = 3.5$ km. The corresponding profiles of the extinction coefficients are shown in Fig. 6*a*. Figure 6*b* depicts the calculated backscattering signals $P(h)$.

To be noted is the fact that, unlike the example of the nonturbid atmosphere (see Fig. 5*b*), not only the level of the lidar signals, but also their relation over the wavelength spectrum changed. It should be expected, and this is confirmed by the calculated results, that height-localized layers of the increased turbidity will be identified more reliably. It is characteristic that such aerosol layers with the optical thickness achieving $\tau = 0.3$ were observed by the SeaWiFS spaceborne module during the powerful earthquake in Gujarat on October 26, 2001 [Ref. 21]. In Fig. 7*a*, the similar situation is simulated by the tenfold increase of the aerosol extinction coefficient in the 1-km layer at the height h = 1.0 km. The results of the corresponding calculations are shown in Fig. 7*b*. It is characteristic that the efficiency of the IR sensing channel increases sharply. This leads to the situation that the spectral behavior of lidar signals changes to the alternative one (Fig. 7*c*). This effect, in our opinion, can serve a qualitative criterion of detection of anomalous aerosol layers of terrigenous origin.

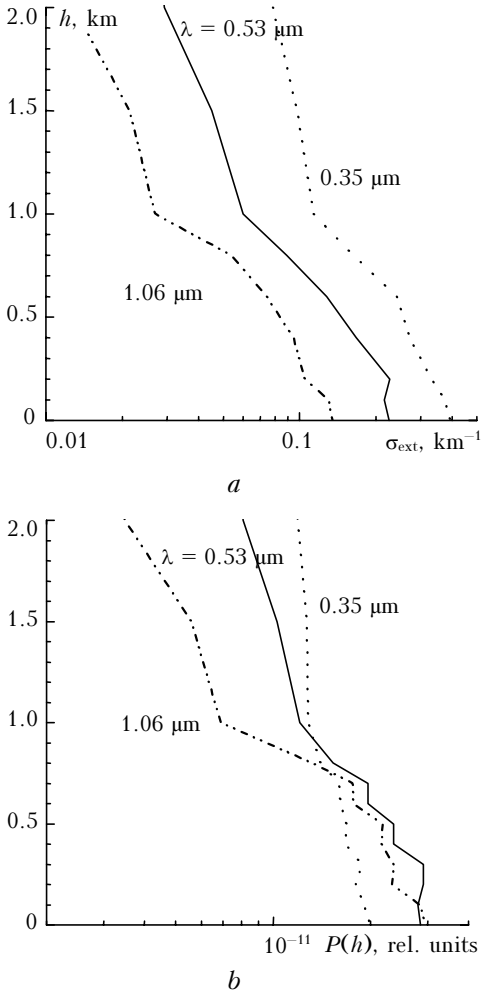

Fig. 6. Results of the numerical experiment on sensing of the boundary atmospheric layer at the increased concentration of aerosol particles: (*a*) model profiles of the extinction coefficients $\sigma(h)$; (*b*) vertical profiles of the lidar signal $P(h)$ for the given wavelengths; detector aperture $\varphi_d = 8.8$ mrad.

However, there arises a question in this situation: how to identify signals reflected by the lower-level clouds and aerosol inversions. The cloudiness is usually characterized by rather high optical density. Comparative results of calculation of the signal $P(h)$ reflected by a cloud, fog, and aerosol inversion are shown in Fig. 7*d*. The extinction coefficient $\sigma(h)$ for a cloud and fog was taken equal to 5 km^{-1}, that is, one of the minimal possible values for liquid-droplet formations.

The calculations have shown that the amplitude of the lidar signal $P(h)$ reflected by a cloud or fog is at least two orders of magnitude higher than that of the signal reflected from an aerosol inversion, even at two- or three-fold increase of its density. However, the spectral dependence of the signal $P(h)$ reflected by the liquid-droplet aerosol is nearly neutral and has no anomalous features. This circumstance is explained by a slight change of the scattering phase function $g(\pi)$ of the cloud aerosol in the given spectral range.

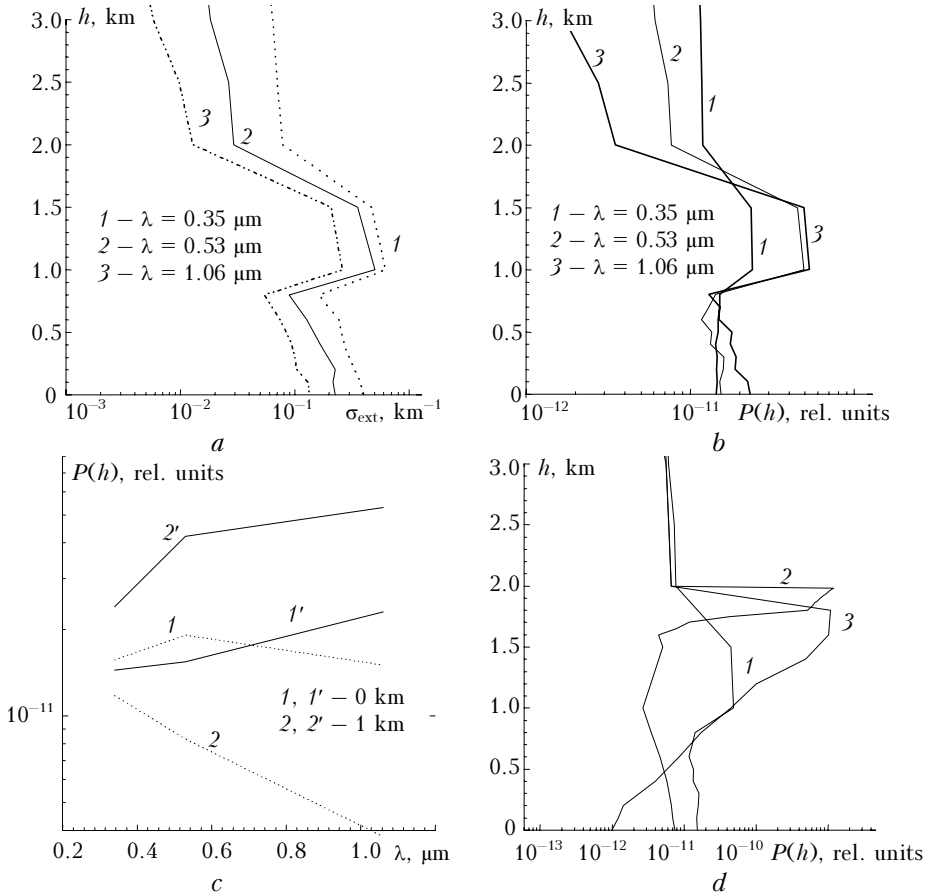

Fig. 7. Results of sensing of an aerosol inversion in the surface atmosphere: (*a*) model profiles $\sigma(h)$; (*b*) vertical profiles $P(h)$; (*c*) spectral behavior of the lidar signal from two height ranges: (*2*, *2*) in and (*1*, *1′*) beyond the inversion zone; (*d*) comparison of signals reflected by an aerosol inversion (*1*), a cloud (*2*) of thickness h = 0.2 km, and a fog layer (*3*) with Δh = 1 km. Calculations are presented for the aperture φ_d = 8.8 mrad.

In addition, at the spaceborne sensing scheme, as was shown in Refs. 55 and 58, the form of the scattering phase function does not play a decisive role in formation of the lidar signal.

It should be also expected that the polarization characteristics of the backscattering signal from liquid-droplet and mineral formations would differ markedly. The anomalous character of the particle size spectrum may serve a decisive criterion for identification of aerosol of seismic and volcanic origins.[19] However, for spaceborne sensing schemes this question calls for additional study.

Conclusions

Measurements of the electric field strength have shown that several hours before an earthquake E begins to increase in the absolute value, while immediately before the earthquake shock it decreases down to background values. The aerosol scattering coefficient before an earthquake increases 1.3–1.5 times, and immediately after the beginning of an earthquake it begins to decrease. The shape and the maximal values of amplitude spectra depend on the time interval between measurements and the shock. Especially wide differences are observed for the spectra of fluctuations of the electric field strength E. It follows from the data obtained that aerosol significantly affects the electric characteristics of the atmosphere. The frequency characteristics of fluctuations of the electric field strength and the aerosol scattering coefficient fall within the frequency range of the Earth's natural oscillations.

The Monte Carlo technique was used to calculate signals of the TECTONICA-A multifrequency orbital lidar designed for detection of aerosol inversions in the atmospheric boundary layer. Estimates are obtained for the wavelengths λ = 1.06, 0.53, and 0.35 μm (three harmonics of the YAG:Nd laser) and the boundary conditions reflecting the actual features of the lidar transceiving system. The basic optical model corresponded to the conditions of the background state on the assumption of stratified inhomogeneity. The model permits the inclusion of aerosol inversions of any origin, natural and anthropogenic. The results obtained allow one to judge the dynamic range of the signal in the given spectral range for different optical situations, in particular, under conditions of aerosol emissions of tectonic origin. Qualitative criteria have been proposed for identification of such emissions by the spectral behavior of reflected signals.

References

1. E. Davies and D.M. Baker, J. Geophys. Res. **70**, No. 9, 2251–2253 (1965).
2. R.S. Leonard and R.A. Barnes, J. Geophys. Res. **70**, 1250–1253 (1965).
3. V.A. Liperovsky, O.A. Pokhotelov, and S.A. Shalimov, *Ionospheric Precursors of Earthquakes* (Nauka, Moscow, 1992), 304 pp.
4. M. Hayakawa, ed., *Atmospheric and Ionospheric Electromagnetic Phenomena Associated with Earthquakes* (Terra Scientific Publ. Comp., Tokyo, 1999), 996 pp.
5. V.N. Strakhov, ed., *Short-Term Prediction of Catastrophic Earthquakes with the Aid of Radiophysical Ground-Based and Space Methods* (OIFZ RAN, Moscow, 1999), 176 pp.
6. S.A. Pulinets and K. Boyarchuk, *Ionospheric Precursors of Earthquakes* (Springer–Verlag, Berlin, 2004), 315 pp.
7. V.I. Larkina, V.V. Migulin, O.A. Molchanov, I.P. Kharkov, A.S. Inchin, and V.B. Schvetcova, Phys. Earth and Planet. Inter. **57**, 100 (1989).
8. V.M. Chmyrev, N.S. Isaev, and S.V. Bilichenko, Phys. Earth Planet. Inter. **57**, 110 (1989).
9. O.A. Molchanov and M. Hayakawa, J. Geophys. Res. A **103**, No. 8, 17489–17504 (2004).
10. A. Krankowski, I.E. Zakharenkova, and I.I. Shagimuratov, Acta Geophys. Pol. **54**, No. 1, 90–101 (2006).
11. I.E. Zakharenkova, I.I. Shagimuratov, A. Krankowski, and A.F. Lagovskii, Issledovano v Rossii, Electron. Journal **110**, 1047–1055 (2006); http://zhurnal.ape.relarn.ru/articles/2006/110.pdf
12. L.S. Ivlev, V.I. Davydova, O.A. Vargas, and A. Martinez, Atmos. Oceanic Opt. **11**, No. 5, 428–431 (1998).
13. A.A. Tronin, Int. J. Remote Sens. **21**, No. 6, 3169–3177 (2000).
14. A.A. Tronin, J. Geodinamics **33**, 519–534 (2002).
15. D. Ouzounov, N. Bryant, T. Logan, S. Pulinets, and P. Taylor, Phys. and Chem. of the Earth **31**, 154–156 (2006).
16. S. Choudhury, S. Dasgupta, and A.K. Saraf, Int. J. Remote Sens. **27**, No. 20, 4381–4396 (2006).
17. L.M. Fishkova and T.I. Toroshelidze, in: *Auroras and Lights of Nocturnal Sky* (Nauka, Moscow, 1989), No. 33, pp. 17–23.
18. http:// www.isprs.org / publication / related / ISPRS/html/papers/526.pdf
19. K.Ya. Kondratyev, L.S. Ivlev, V.F. Krapivin, and C.A. Vaortsos, *Atmospheric Aerosol Properties* (Springer Praxis Publ., Chichester UK, 2006), 622 pp.
20. S. Dey, S. Sarkar, and R.P. Singh, Adv. Space Res. **33**, No. 3, 274–278 (2004).
21. Y. Okada, S. Mukai, and R.P. Singh, Adv. Space Res. **33**, No. 3, 254–258 (2004).
22. Z. Shou and D. Harrington, Geophys. Res. Abstr. **7**, 02175 (2005).
23. Quang Zuji and Du Le-Tian, Earth Sci. Front. **8**, No. 2, 235–345 (2001).
24. V.A. Liperovsky, C.V. Meister, E.V. Liperovskaya, and V.F. Davidov, Natur. Hazards and Earth System Sci. **5**, 783–789 (2005).
25. M.A. Dunajecka and S.A. Pulinets, Atmosfera **18**, No. 4, 235–247 (2005).
26. V.V. Lasukov, Izv. Vyssh. Uchebn. Zaved. Fiz., No. 2, 69–75 (2000).
27. S. Pulinets, Technol. Abber. Optimigation **15**, No. 3, 413–435 (2004).
28. L.I. Morozova, Izv. Ros. Akad. Nauk. Fiz. Zemli, No. 5, 65–67 (1997).
29. M. Hayakawa, ed., *Seismo-Electromagnetics: Litosphere–Atmosphere–Ionosphere Coupling* (TERRPUB, Tokyo, 2002), 477 pp.
30. V.M. Zakharov, O.K. Kostko, and S.S. Khmelevtsov, *Lidars and Investigations of Climate* (Gidrometeoizdat, Leningrad, 1990), 319 pp.
31. W. Renger, C. Kieme, H.-G. Schreiber, M. Wirth, and P. Moerl, in: *Final Results Workshop Proc. IROE-CNR, Florence, Italy* (1995), pp. 15–19.
32. V.S. Shamanaev, Atmos. Oceanic Opt. **6**, No. 2, 101–103 (1993).
33. P. Parvin, G.R. Davoud-Abadi, and H. Kariminezhad, in: *23-th Int. Laser Radar Conf. Proc. (*Nara, Japan, 2006), pp. 245–247.
34. V.G. Bondur and A.T. Zverev, Issled. Zemli iz Kosmosa, No. 3, 37–52 (2005).
35. V.E. Zuev, G.M. Krekov, and I.E. Naats, Acta Astronaut. **1**, 93–103 (1974).
36. V.M. Zakharov, ed., *Laser Sensing of the Atmosphere from Space* (Gidrometeoizdat, Leningrad, 1988), 213 pp.
37. Y.S. Balin, V.V. Burkov, and I.V. Znamenskii, in: *15th Int. Laser Radar Conf. Abstracts* (Tomsk, USSR, 1990), pp. 12–13.
38. M.P. McCormick, D.M. Winker, and E.V. Browell, Bull. Am. Meteorol. Soc. **74**, 205–214 (1993).
39. Yu.S. Balin, A.A. Tikhomirov, and S.V. Samoilova, Atmos. Oceanic Opt. **10**, No. 3, 209–220 (1997).
40. G.G. Matvienko, G.P. Kokhanenko, V.S. Shamanaev, and V.A. Alekseev, in: *Int. Symp. Remote Sens. Conf. Abstracts* (Barcelona, Spain, 1998), pp. 37–38.
41. G.G. Matvienko, G.M. Krekov, V.A. Alekseev, Ju. Polushkovskii, and G.M. Chernjavskii, in: *36th Sci. Assembly of COSPAR Abstracts* (Beijing, China, 2006), p. 147.
42. G.M. Krekov, M.M. Krekova, and G.G. Matvienko, Atmos. Oceanic Opt. **13**, No. 8, 677–684 (2000).
43. http://www.iki.rssi.ru/earth/trudi/1-25.pdf
44. V.A. Alekseev, N.G. Alekseeva, and Ya.D. Murav'ev, Dokl. Ros. Akad. Nauk **345**, No. 5, 667–670 (1995).
45. V.A. Alekseev and N.G. Alekseeva, Nucl. Geophys. **6**, No. 1, 99–110 (1992).
46. V.A. Donchenko, Atmos. Oceanic Opt. **2**, No. 1, 1–12 (1989).
47. R.V. Andreson and R.E. Larson, J. Geophys. Res. **79**, No. 24, 3432–3435 (1974).
48. E.T. Pierce, Geophys. Res. Lett. **3**, No. 3, 185–188 (1976).
49. V.A. Alekseev, N.G. Alekseeva, and J. Ichankuliev, Radiat. Measurem. **25**, Nos. 1–4, 637–639 (1995).
50. E.T. Pierce, Geophys. Res. Lett. 3, No. 3, 185–188 (1976).
51. J.S. Bendat and A.G. Pearsol, *Random Data: Analysis and Measurement Procedures* (Wiley–Interscience, New York, 1971).
52. G.A. Chalmers, *Atmospheric Electricity* (Pergamon, Oxford, 1967).
53. L.M. Shvarts and L.V. Oguryaeva, Meteorol. Gidrol., No. 7, 59–64 (1987).
54. V.A. Alekseev and A. Lyash, in: *Proc. of 2nd Int. Conf. on Small Satellites, New Technologies, Microminiaturization* (Korolev, Russia, 1999), pp. 1–15.
55. G.M. Krekov, M.M. Krekova, and I.V. Samokhvalov, Issled. Zemli iz Kosmosa, No. 6, 77–83 (1986).
56. G.M. Krekov, S.I. Kavkyanov, and M.M. Krekova, *Interpretation of Signals of Optical Sensing of the Atmosphere* (Nauka, Novosibirsk, 1987), 173 pp.
57. V.E. Zuev and G.M. Krekov, *Optical Models of the Atmosphere* (Gidrometeoizdat, Leningrad, 1986), 256 pp.
58. G.M. Krekov and M.M. Krekova, Atmos. Oceanic Opt. **11**, No. 1, 42–45 (1998).